Journal of Power Sources 196 (2011) 6573–6582

Contents lists available at ScienceDirect

Journal of Power Sources

journal homepage: www.elsevier.com/locate/jpowsour

Inhibitive action of ferricyanide complex anion on both corrosion and passivation of zinc and zinc–nickel alloy in the alkaline solution

Abdel-Rahman El-Sayed*, Hossnia S. Mohran, Hany M. Abd El-Lateef

Chemistry Dept., Faculty of Science Sohag, 82524, Sohag University, Egypt

ARTICLE INFO

Article history:
Received 11 October 2010
Received in revised form 10 February 2011
Accepted 27 March 2011
Available online 6 April 2011

Keywords:
Corrosion
Inhibition
Zinc
Zn–Ni alloy
Ferricyanide
Alkaline solution

ABSTRACT

The corrosion of zinc and Zn–0.5Ni alloy in strong alkaline solution (7 M KOH) in the absence and presence of $[Fe(CN)_6]^{3-}$ complex anion (1×10^{-3}–1×10^{-2} M) as inhibitor has been studied. Tafel plot, potentiodynamic, potentiostatic and electrochemical impedance spectroscopy (EIS) techniques were used, and complementary by EDX and SEM investigation. It is observed that, the corrosion current density (I_{corr}) decreases, and the inhibition efficiency (*IE*%) increases as the concentration of inhibitor is increased. The shift of breakdown potential to less positive direction, indicating that the reduction of oxide layer on the alloy surface occurs somewhat easier in the presence of $[Fe(CN)_6]^{3-}$ complex anion. The impedance measurements have shown that the increase of the inhibitor concentration in the alkaline solution reduces the corrosion rate in the active region. Accordingly, addition of $[Fe(CN)_6]^{3-}$ complex anion to KOH solution can be considered as an important criteria for a good battery anodes. This behavior is due to its high negative open-circuit potential, less corrosion rate and higher self-catalysis in the passive region compared with those in its absence.

1. Introduction

Zinc is a favorable anode in primary batteries because of its high capacity, high discharge efficiency and high safety features associated with its manufacturing process and use [1]. Zinc has been added with mercury to suppress the evolution of hydrogen gas brought on by the self-discharge reactions of zinc and by the increase in internal cell impedance [2–15]. The use of mercury has become an environmental issue and the attention has been focused on developing mercury-free batteries. In general, either zinc or its alloys are used as anodes in these batteries. The purity of the zinc is very high, i.e. of the order of 99.9 wt.% or more. Hence, the development of zinc or zinc-based alloys as anodes for alkaline power sources has become a necessity and in this connection, development of mercury-free zinc assumes great importance. Similarly, Zn-air battery technology also requires mercury-free zinc anodes. As it is known, Zn corrosion in alkaline solution is cathodic controlled, so the rate of the cathodic hydrogen evolution limits the Zn corrosion rate. Hence the best way to slow down the corrosion process is to reduce the hydrogen evolution rate, which can be achieved by the introduction of a small amount of other metals as Bi, Pb, Al and In into Zn [16]. Recently, the authors [17] were added small amount from Ni (0.5%) to zinc in order to improve the electrochemical behavior of the discharge cell, and to suppress the anodic reaction of zinc. However, still there is a need to add another component to the electrolyte which is capable of reducing the corrosion of zinc or its alloy in alkaline solution. Therefore, the present work was undertaken to study the role of $[Fe(CN)_6]^{3-}$ complex anion on the corrosion and electrochemical behavior of zinc and its alloy (0.5% Ni) in 7 M KOH solution. Potassium ferricyanide has very low toxicity, it can be safe in alkaline solution, and it is used as an oxidizing agent. Careful examination of the literature reveals that the studied $[Fe(CN)_6]^{3-}$ complex anion has not yet been studied as corrosion inhibitor of zinc or its alloys. However, some papers only appeared dealing with $[Fe(CN)_6]^{3-}$ complex anion as corrosion inhibitor for iron electrodes of batteries in alkaline solution [18–22].

2. Experimental

2.1. Materials and solutions

7 M solution of KOH (analytical grade) was prepared by dissolving the appropriate weight in doubly distilled water. Potassium ferricyanide was purchased from Merck. The solution was prepared by dissolving the appropriate amount by weight in doubly distilled water (at concentration range 10^{-3}–10^{-2} M). The desired volume of the inhibitor solution was added to the electrolyte. Zn and Ni

* Corresponding author. Tel.: +20 934601159; fax: +20 934601159.
E-mail addresses: elsayed777@yahoo.com (A.-R. El-Sayed), Hossniamohran@yahoo.com (H.S. Mohran), Hany_shubra@yahoo.co.uk (H.M. Abd El-Lateef).

0378-7753/$ – see front matter © 2011 Elsevier B.V. All rights reserved.
doi:10.1016/j.jpowsour.2011.03.057

of high purity (99.999%; Johnson Matthey Chemicals Ltd.) were used to prepare Zn–Ni alloy as disk electrodes ($A = 0.196\,cm^2$) in a Gallenkamp muffle furnace using evacuated closed silica tubes at 1000 °C for 24 h. The melts were shaken every 6 h to ensure the homogeneity of melting alloy and finally the melts were quenched in an ice as previously discussed [23]. One Zn–Ni alloy was prepared with the composition of 99.5%Zn–0.5%Ni alloy. Analysis of Zn–0.5Ni alloy using X-ray diffraction and SEM showed that the alloy contains γ-Zn_3Ni phase dispersed in Zn-matrix [17].

The prepared alloy was analyzed using X-ray photoelectron spectroscopy. For the alloy, the percentage of Zn and Ni was found in accordance with the percentage of mixing Zn and Ni. The microhardness of Zn and prepared Zn–Ni alloy was measured using a Leiz Wetzlar Microhardness tester with a Vickers diamond pyramid indicator; a load of 100 g was used, and the microhardness was expressed in kilograms per square millimeter.

2.2. Electrochemical measurements

The measurements were performed on planar disk electrode embedded in an Araldite holder. Prior to each measurement the electrodes were polished with sequacious grades of emery paper, degreased in pure ethanol and washed in running bidistilled water before being inserted in the polarization cell. The reference electrode was a saturated calomel electrode (SCE) to which all potentials are referred.

The cell description is given elsewhere [24]. To remove any surface contamination and air formed oxide, the working electrode was kept at −1.5 V (SCE) for 5 min in the tested solution, disconnected shaken free of adsorbed hydrogen bubbles and then cathodic and anodic polarization was recorded. Potentiostat/Galvanostat (EG&G Model 273) connected with a personal computer (IBM Model 30) was used for the measurements.

2.2.1. Tafel polarization technique

The extrapolation of cathodic and anodic Tafel lines was carried out in a potential range ±0.20 V with respect to corrosion potential (E_{corr}) at scan rate of 1 mV s^{-1} using software version 342C supplied from EG&G Princeton Applied Research.

2.2.2. Potentiodynamic technique

The potentiodynamic polarization studies were carried out with electrodes having a surface area of 0.196 cm^2. The potential was altered automatically from the steady state open circuit potential (E_{corr}) up to +1.0 V vs. SCE and at a scan rate of 1 mV s^{-1} using software version 342C Supplied from EG&G Princeton Applied Research.

2.2.3. Potentiostatic technique

The anodic potential was fixed at a required constant value and the variation of current density was recorded as a function of time (current density–time transients).

2.2.4. Electrochemical impedance spectroscopy (EIS)

Electrochemical impedance spectroscopy (EIS) measurements were performed with a phase-sensitive detector (amplifier) (Model 5208) driven by a potentiostat/galvanostat apparatus (model 273) from EG&G Instruments. The electrochemical software of this Model is 378. The EIS measurements were acquired at steady of state open circuit potential (E_{corr}) in the frequency range from 100 kHz to 5 MHz. Amplitude of 5 mV peak to peak was used for the ac signal for all EIS measurements.

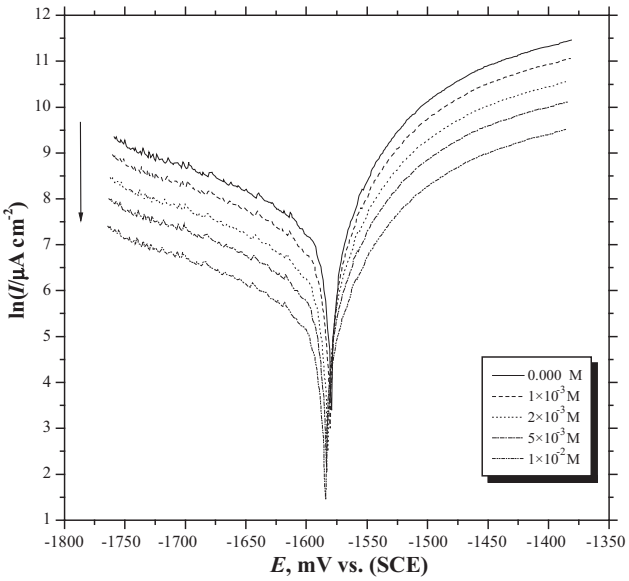

Fig. 1. Tafel polarization curves for pure Zn in 7 M solution of KOH containing various concentrations of $K_3[Fe(CN)_6]$ at 25 °C.

2.3. Surface analysis

The composition and morphology of the corrosion products formed on the surface of electrodes in 7 M KOH solutions in the absence and presence of $[Fe(CN)_6]^{3-}$ complex anion were tested at applied potential −0.50 V vs. SCE by using energy-dispersive X-ray spectroscopy analysis (EDX) conducted with scanning electron microscope (SEM) (SEM-EDX) (JEOL, model 5300).

2.4. Methods of evaluation of corrosion parameters

Steady state of open circuit corrosion potential (E_{corr}) for the investigated electrodes in the absence and presence of the studied inhibitor was attained after 60–70 min from the moment of immersion. Corrosion current density (I_{corr}) of the investigated electrodes was determined by Abdel Aal et al. [25] by extrapolation of cathodic and anodic Tafel lines to corrosion potential (E_{corr}).

The inhibition efficiency expressed as percent inhibition (*IE*%) is defined as

$$IE\% = \frac{I_{uninh.} - I_{inh.}}{I_{uninh.}} \times 100 \quad (1)$$

where $I_{uninh.}$ and $I_{inh.}$ are the uninhibited and inhibited corrosion currents. The inhibited corrosion currents are those determined in the presence of the studied compound used in this investigation and can be considered as corrosion inhibitor. The uninhibited corrosion currents were determined in pure (inhibitor free) 7 M KOH at the same temperature.

3. Results and discussion

3.1. Extrapolation of cathodic and anodic Tafel lines

Figs. 1 and 2 show the influence of $[Fe(CN)_6]^{3-}$ complex anion concentration on the Tafel cathodic and anodic polarization characteristics of both pure zinc and its alloy (0.5%Ni) in 7 M KOH solution of scan rate 1 mV s^{-1} and at 25 °C. Corrosion parameters were calculated on the basis of cathodic and anodic potential versus current density characteristics in the Tafel potential region [26,27]. The values of the corrosion current density (I_{corr}) for the investigated metal and its alloy without and with the inhibitor, respectively

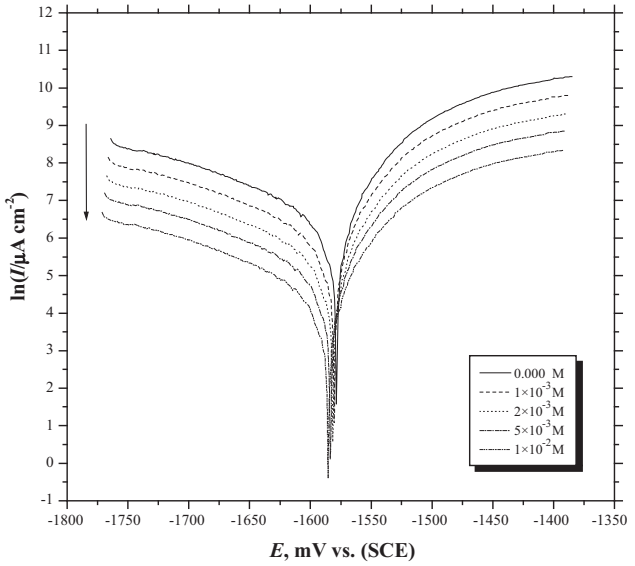

Fig. 2. Tafel polarization curves for pure Zn–0.5Ni alloy in 7 M solution of KOH containing various concentrations of $K_3[Fe(CN)_6]$ at 25 °C.

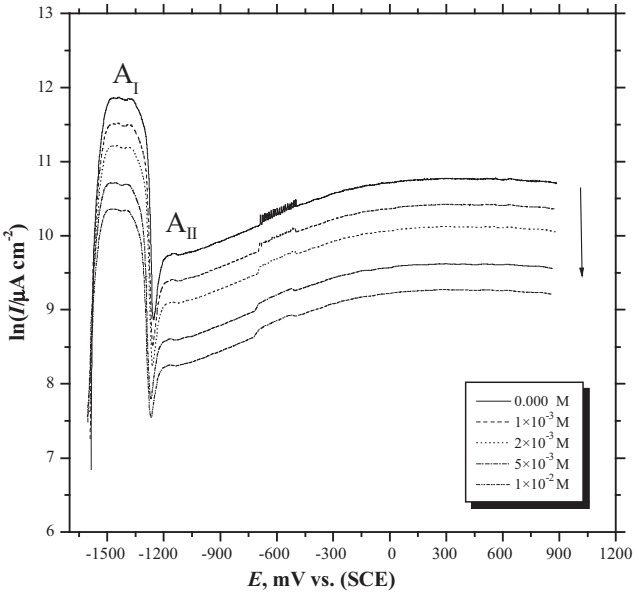

Fig. 3. Potentiodynamic anodic polarization curves for pure Zn in 7 M solution of KOH containing various concentrations of $K_3[Fe(CN)_6]$ at 25 °C.

were determined by the extrapolation of cathodic and anodic Tafel lines to the corrosion potential (E_{corr}). It can be seen that the presence of $[Fe(CN)_6]^{3-}$ complex anion results a marked shift in both cathodic and anodic branches of the polarization curves towards lower current densities. This means that, the inhibitor affects both cathodic and anodic reactions. Also, slight negative shift in the corrosion potential (E_{corr}) is observed. The results showed that the inhibiting action of $[Fe(CN)_6]^{3-}$ complex anion on the both cathodic and anodic processes seems to approximately be equal. The inhibitor may decrease the corrosion through the reduction of zinc or its alloy reactivity. Accordingly to this mechanism, a reduction of either the anodic or the cathodic reaction or both arises from the adsorption of the inhibitor on the corresponding active sites [28].

The data in Table 1 exhibited that the corrosion current density (I_{corr}) decreases, and the inhibition efficiency (*IE*%) increases as the concentration of inhibitor is increased. These results suggest that retardation of the electrodes processes occurs, at both cathodic and anodic sites, as a result of coverage of these sites by $[Fe(CN)_6]^{3-}$ complex anion. However, the inhibition efficiency (*IE*%) in the case of alloy is higher than that of pure zinc at the same examined concentrations. This indicates the inhibitor interacts more favorably with the alloy surface than that with pure zinc [29]. The increase of inhibitor efficiency with increasing the concentration can be interpreted on the basis the adsorption amount and the coverage of $[Fe(CN)_6]^{3-}$ complex anion, increases with increasing concentration [30]. On the other hand, the steady state open circuit potential slightly shifts to more negative values, and the shift increases with increasing the concentration of $[Fe(CN)_6]^{3-}$ complex anion of both pure zinc and its investigated alloy. This indicates that the changes in potential of hydrogen evolution towards more negative values in the presence of the inhibitor have a positive effect on charge efficiency and self-discharge [17].

The fact that the slopes of the cathodic (b_c) and anodic (b_a) Tafel lines in Table 1 remain almost unchanged upon addition of the inhibitor. These results indicate that this inhibitor acts by simply blocking the available surface area. In other words, the inhibitor decreases the surface area for corrosion of the investigated metal and its alloy, and only causes inactivation of a part of the surface with respect to corrosive medium [31].

3.2. Potentiodynamic polarization curves

Figs. 3 and 4 show the potentiodynamic anodic polarization curves of zinc and its alloy (Zn–0.5Ni alloy) in 7 M KOH solution containing various concentrations of $[Fe(CN)_6]^{3-}$ complex anion at scan rate 1 mV s^{-1} and at 25 °C. The polarization curves were swept from the steady state of open circuit potential (E_{corr}) up to +1.0 V vs. SCE. The anodic polarization curves exhibit an active/passive transition in the case of pure zinc and its investigated alloy. In the active region, the dissolution current increases linearly with the applied potential, then followed by the appearance of two peaks (A_I and A_{II}). However, the two peaks in the case of pure zinc are appeared at more negative potentials than those of the alloy. As mentioned in our previous work [17] that in the case of pure zinc, the broad peak A_I is well defined at about −1.39 V vs. SCE in 7 M KOH solution,

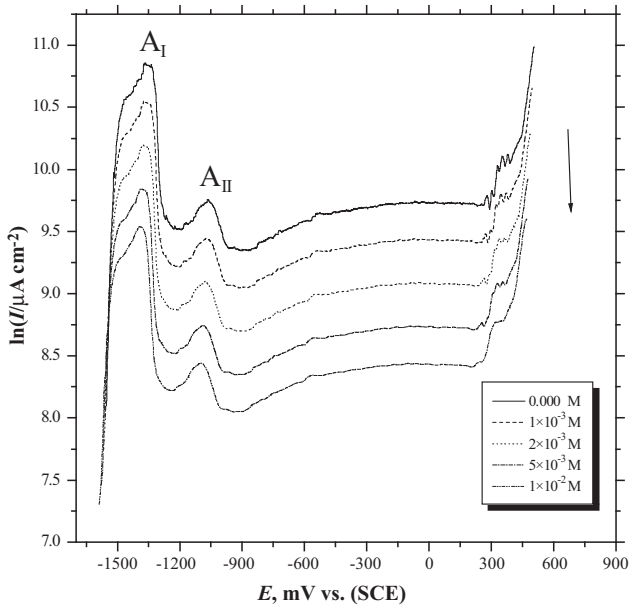

Fig. 4. Potentiodynamic anodic polarization curves for Zn–0.5Ni alloy in 7 M solution of KOH containing various concentrations of $K_3[Fe(CN)_6]$ at 25 °C.

Table 1
Corrosion parameters obtained from Tafel polarization for pure Zn and Zn–0.5Ni alloy in 7 M solution of KOH containing various concentrations of $K_3[Fe(CN)_6]$ at 25 °C.

Metal and alloy	Concentration (mol/l)	$-E_{corr}$ (mV)	I_{corr} (mA/cm^2)	IE (%)	b_a (mV)/decade	$-b_c$ (mV)/decade	α
Zn	0.0	1578	1.096	–	75	111	0.54
	1×10^{-3}	1580	0.823	25.0	76	110	0.54
	2×10^{-3}	1581	0.558	49.5	76	110	0.54
	5×10^{-3}	1583	0.372	65.2	76	110	0.54
	1×10^{-2}	1585	0.21	81.0	76	110	0.54
Zn–0.5Ni alloy	0.0	1581	0.492	–	84	127	0.46
	1×10^{-3}	1583	0.354	27.5	86	128	0.46
	2×10^{-3}	1585	0.221	55	86	128	0.47
	5×10^{-3}	1586	0.145	70.5	86	127	0.47
	1×10^{-2}	1588	0.074	85.1	86	127	0.47

and can be related to the formation of $Zn(OH)_2$. While small anodic peak A_{II} appearing at about −1.081 V vs. SCE, and may be related to dehydration of $Zn(OH)_2$ to ZnO. Under the same conditions, the anodic polarization curves of Zn–0.5Ni alloy exhibited peak (A_I) at about −1.295 V vs. SCE which can be associated with the electroformation of ZnO film. While the second peak (A_{II}) appearing at about −0.98 V vs. SCE, which is related to the formation of $Ni(OH)_2$. X-ray diffraction was confirmed the formation of these oxides or hydroxides at the mentioned peaks potentials [17].

The effect of the addition of different concentrations of $[Fe(CN)_6]^{3-}$ complex anion as a potassium salt on the potentiodynamic response for zinc and its alloy in 7 M KOH solution was examined. The curves in Figs. 3 and 4 show that an increase in the inhibitor concentration causes gradually decrease in the height of peaks (I_{peak}) as well as the passivation current (I_{pass}) and shifts peak potentials (E_{peak}) to more negative direction. This means that an increase in the inhibitor concentration enhances the adsorption of the inhibitor anions, and hence decreases the peak and passivation current densities. This exhibits that $[Fe(CN)_6]^{3-}$ complex anion has ability to adsorb and block the active dissolution sites on the electrode surface of both Zn and its alloy. On the other hand, the data display that the presence of any concentration of the investigated complex anion shifts the peak potentials (E_{peak}) to more negative direction, indicating that the investigated anions are strongly adsorbed on the electrode surface act as effective inhibitor. Consequently, this behavior can be attributed to the competitive adsorption of the inhibitive anions with OH^- ions on the surface, thus preventing OH^- ions from attack the metal or alloy surface. In the same time, the decrease in the passivation current (I_{pass}) with increasing the concentration of the inhibitor can be interpreted on the basis that the passive layer consists from $Zn(OH)_2$ and ZnO in the case of zinc, and ZnO and NiO in the case of Zn–0.5Ni alloy. Consequently, the dissolving power of OH^- ions on the passive layer decreases in the presence of $[Fe(CN)_6]^{3-}$ complex anion, due to its adsorption on the surface. El-Sayed [22] studied the effect of $[Fe(CN)_6]^{3-}$ complex anion on the electrochemical and corrosion behavior of iron and sintered iron electrodes in the alkaline solution. He assumed that ferric hydroxide precipitate from the complex, thus blocking pores and decreasing the activity of the electrode. In general, the effect of $[Fe(CN)_6]^{3-}$ complex anion on the electrochemical behavior of both zinc and its investigated alloy, can be attributed to the redox couple $[Fe(CN)_6]^{3-}/[Fe(CN)_6]^{4-}$ which is of particular interest, since it involves ionic species carrying a large negative charge. Formation of slightly soluble species from ferri- and ferro-cyanide is reported by Kawiak et al. [20]. They stated that, the decrease in the electrode activity in the presence of mentioned complex possibly arises from a partial blocking of the electrode surface by precipitating complex. General agreement was found with the results of Moshtev [32] and Oimedo et al. [21]. They characterized the redox reaction of ferri, ferrocyanide on passive iron in alkaline solution. Although, it is impossible to identify this compound, it can be assumed that it is formed by Zn^{2+} or Ni^{2+} ions produced at the investigated electrodes. Adsorption of $Zn(CN)_2$ or $Ni(CN)_2$ was suggested, since the ratio for the two cations to CN^- was near 1:2. However, adsorption species are more complex than $[Fe(CN)_6]^{3-}$ and $[Fe(CN)_6]^{4-}$. Possibly both cyanide complexes take part in the formation reaction of the precipitate.

Fig. 5 shows the relationship between the breakdown potential ($E_{breakdown}$) and the concentration of the investigated inhibitor. It is observed that the breakdown potential of the oxide film formed on the alloy surface ($E_{breakdown}$) shifts to less positive potential with increasing the concentration of $[Fe(CN)_6]^{3-}$ complex anion. These results suggest that the inhibitor is preferentially adsorbed on the alloy surface thereby hindering oxide growth. Accordingly, the reduction of the oxide layer at the alloy surface occurs somewhat easier in the presence of the investigated inhibitor. Therefore, the addition of $[Fe(CN)_6]^{3-}$ complex anion to alkaline solution, promotes the electrochemical reaction of the investigated alloy in the passive region, contributes to suppression of hydrogen gas evolution and inhibits the corrosion rate. In addition, the alloy surface is reactivated in the passive region.

3.3. Potentiostatic measurements

In order to establish that the current density decreases as a result of oxide film formed at both peaks and more positive potentials. Potentiostatic measurements are examined. Figs. 6 and 7 show

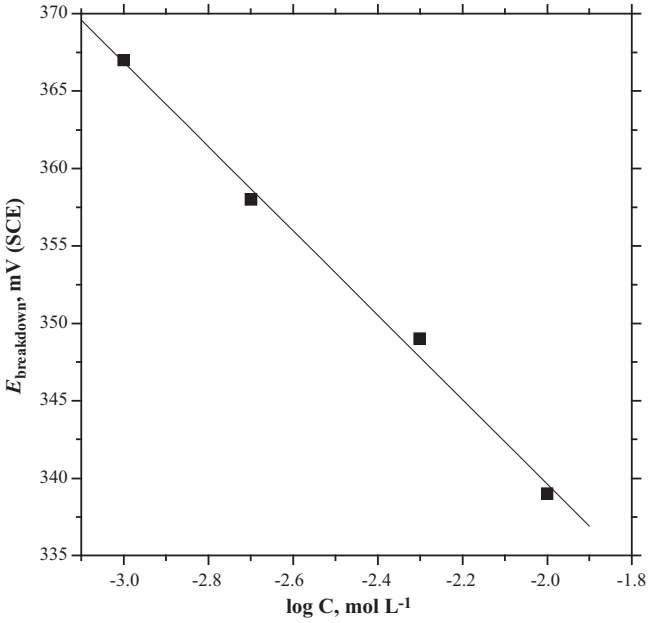

Fig. 5. Dependence of the breakdown potential E_b on the concentration of $K_3[Fe(CN)_6]$ for Zn–0.5Ni alloy in 7 M KOH solution at 25 °C.

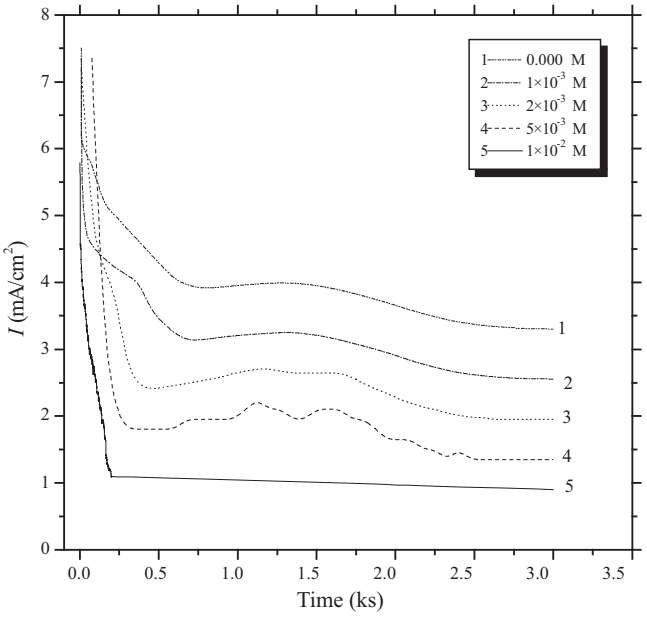

Fig. 6. Potentiostatic transient's current vs. time curves for pure Zn in 7 M KOH solution containing various concentrations of $K_3[Fe(CN)_6]$ at peak A_I (−1.311 V vs. SCE) and at 25 °C.

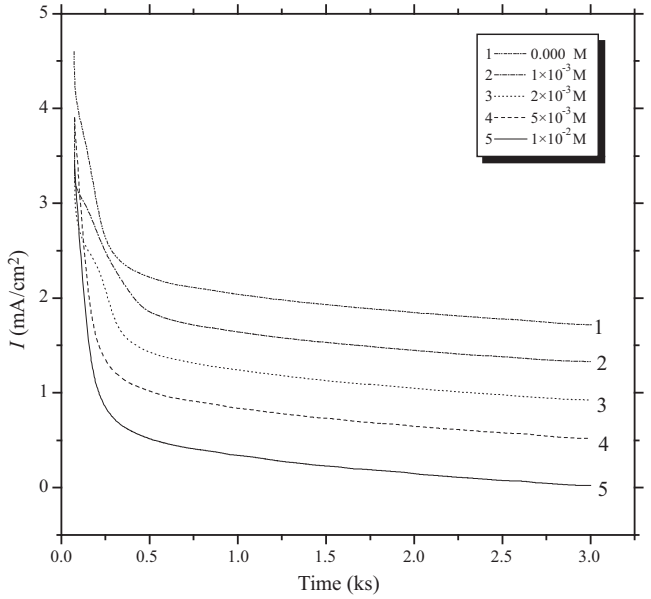

Fig. 8. Potentiostatic transient's current vs. time curves for pure Zn in 7 M KOH solution containing various concentrations of $K_3[Fe(CN)_6]$ at passive region (+1.0 V vs. SCE) and at 25 °C.

the current–time transient curves of Zn and its alloy in 7 M KOH solution containing various concentrations of $[Fe(CN)_6]^{3-}$ complex anion at peak potential, A_I (at −1.311 V vs. SCE in the case of zinc and at −1.285 V vs. SCE in the case of alloy). Generally, it is observed that the current density decreases with time. However, the effect of adding increasing concentration of $[Fe(CN)_6]^{3-}$ complex anion, exhibited that the current density decreases gradually with increasing the concentration. This behavior confirmed that this anion function as inhibitor [33]. These results agree with those obtained from potentiodynamic measurements. This behavior is believed to be associated with the ability of $[Fe(CN)_6]^{3-}$ complex anion to adsorb and block the active dissolution sites on the investigated electrodes surfaces. The inorganic complex anions can adsorb on the surface and dislodge the OH^- anions and thereby retard the active dissolution.

Figs. 8 and 9 represent the current–time transient curves under the effecting of adding the investigated inhibitor at the passive region (at +1.0 and 0.0 V vs. SCE of Zn and alloy, respectively). By comparing the steady state values of current density, it is observed that this value of current density decreases with increasing the concentration of the mentioned inhibitor. This behavior could be explained in terms of the oxide film theory of passivity proposed by Hoar et al. [34] due to the penetration of the inhibitive anion through the oxide film on the surface, contaminating, thereby, favoring passive growth. Consequently, this behavior may be attributed to the competitive adsorption of the inhibitive anions with OH^- ion on the electrode surface. Thus preventing

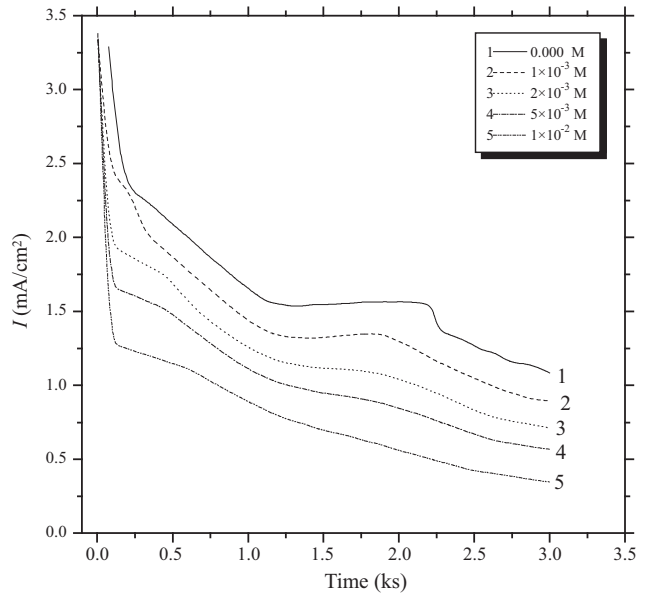

Fig. 7. Potentiostatic transient's current vs. time curves for Zn–0.5Ni alloy in 7 M KOH solution containing various concentrations of $K_3[Fe(CN)_6]$ at peak A_I (−1.285 V vs. SCE) and at 25 °C.

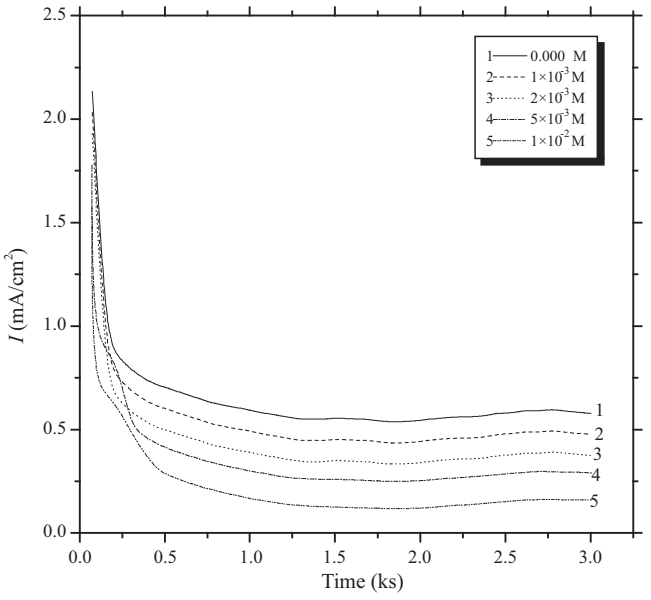

Fig. 9. Potentiostatic transient's current vs. time curves for Zn–0.5Ni alloy in 7 M KOH solution containing various concentrations of $K_3[Fe(CN)_6]$ at passive region (+0.0 V vs. SCE) and at 25 °C.

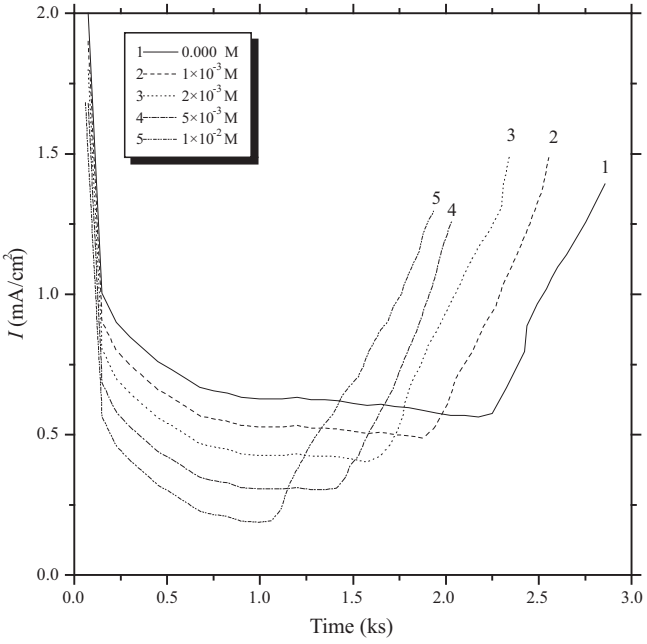

Fig. 10. Potentiostatic transient's current vs. time curves for Zn–0.5Ni alloy in 7 M KOH solution containing various concentrations of $K_3[Fe(CN)_6]$ at breakdown potential (+0.425 V vs. SCE) and at 25 °C.

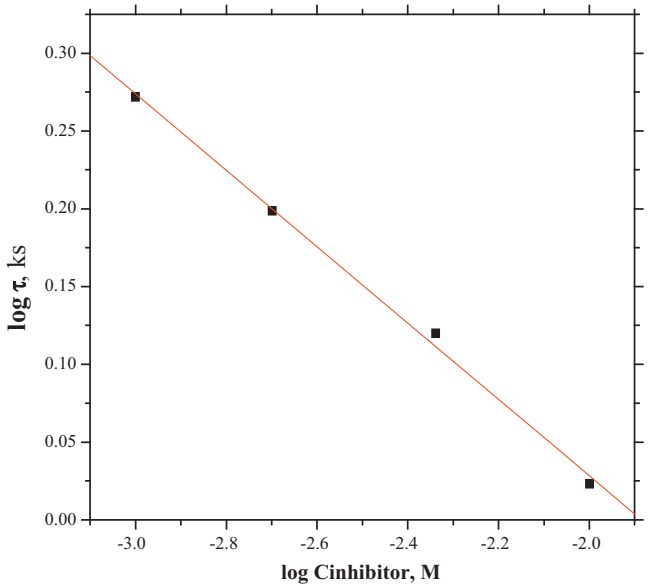

Fig. 11. Linear dependence of log time breakdown vs. log $C_{inhibitor}$ for Zn–0.5Ni alloy in 7 M KOH solution at +0.425 V vs. SCE and 25 °C.

the OH^- ion from sites through which it preferentially adsorbs on the protective film, and therefore decrease the tendency for the dissolving oxide film.

Fig. 10 shows the variation of current density with time of Zn–0.5Ni alloy at certain positive potential (breakdown potential). It is observed that the current density initially decreases gradually with time. This indicates that oxides of Zn and Ni are formed on the alloy surface and the current flowing at this time may correspond to film formation, and repairing the film materials [35]. However, after certain time of imposed potential, the current density rises suddenly. This proves that the oxide film formed on the alloy surface tends to breakdown and reactivation of the alloy surface takes place at certain positive potential (+0.425 V vs. SCE) [36]. On the other hand, it is observed that, the breakdown time ($t_{breakdown}$), decreases with increasing the concentration of the inhibitor. This behavior may be attributed to the adsorption of $[Fe(CN)_6]^{3-}$ complex anion on the surface, increasing the solubility of oxides and peptization of the passive film. The relation between the two variables is best represented by plotting them on a double logarithmic scale (Fig. 11), where a straight line relation is observed as is satisfactory represented by the equation:

$$\frac{\log \ t_{breakdown}}{K_s} = a - b \ \log \ C_{inh.} \tag{2}$$

where a and b are constant. As mentioned before in our previous work [17] that the breakdown of the passive film formed on the alloy surface in the same mentioned concentration of KOH solution, as due to that some Ni(II) is precipitated in ZnO lattice. Consequently, when $[Fe(CN)_6]^{3-}$ complex anions adsorb on the oxide layer, there is a tendency of the inhibitor ions to interact with Ni(II) may be to form soluble complex diffuses to the bulk of the solution. This behavior leads to creating defects in the passive layer. The adsorption of $[Fe(CN)_6]^{3-}$ complex anions at this certain positive potential increases the potential difference across the passive film which enhances the rate of diffusion of Ni(II) ions from the alloy/film interface to the film/solution interface. Consequently to the formation of cation vacancies takes place, which lead in turn to breakdown of the passive film [37]. Accordingly, the breakdown of the passive layer becomes easier in the presence of the inhibitor anion and increases with increasing the concentration. Therefore, one can conclude that, the time required to breakdown the oxide layer at certain positive potential of Zn–0.5Ni alloy decreases with increasing the concentration. Accordingly, this inhibitor has a beneficial effect as self-catalysis for the studied alloy which can be used as anode in alkaline storage batteries, and restores its activity again.

3.4. Electrochemical impedance spectroscopy measurements (EIS)

In order to support the data obtained from extrapolation of cathodic and anodic Tafel lines, electrochemical impedance spectroscopy (EIS) of Zn and its investigated alloy in 7 M solution of KOH containing various concentrations of $[Fe(CN)_6]^{3-}$ complex anion is examined. The complex plane of impedance at E_{corr} is plotted as shown in Figs. 12 and 13. An analysis of the impedance at the examined potential was made. The data of the charge transfer resistance, R_{ct}, and the capacity of the double layer (C_{dl}) were calculated using both Nequist and Bode plots of the impedance spectrum (Table 2). However, the Warburg impedance (Z_w) is determined from the following equations [38]:

$$Z^{/} = \sigma \frac{1}{\omega^{1/2}} - j\frac{\sigma}{\omega^{1/2}} \tag{3}$$

$$|Z^{/}| = \frac{\sqrt{2}\sigma}{\omega^{1/2}} \tag{4}$$

The Warburg coefficient, σ, can be determined from the slope of the Warburg plot (the slope of real parts of $Z^{/}$ vs. $1/\omega^{1/2}$; $\omega = 2\pi F$), or by fitting to an equivalent circuit model which includes a Warburg impedance. However, most equivalent circuit modeling programs return "Z_w" rather than σ, Z_w is the Warburg impedance ($Z_w = W$) which are calculating from the following equation (Table 2):

$$\sigma = \frac{1}{Z_w\sqrt{2}} \tag{5}$$

The recorded spectra show one capacitive loop at the higher frequency range (HF) followed by the Warburg Tail at lower frequency values (LF) (Figs. 12 and 13). The curves in Figs. 12 and 13 exhibit that Z_w is the Warburg impedance, related to the diffusion of soluble species from the electrode surface to the bulk of solution [39,40]. The diameter of the capacitive loop R_{ct}, and War-

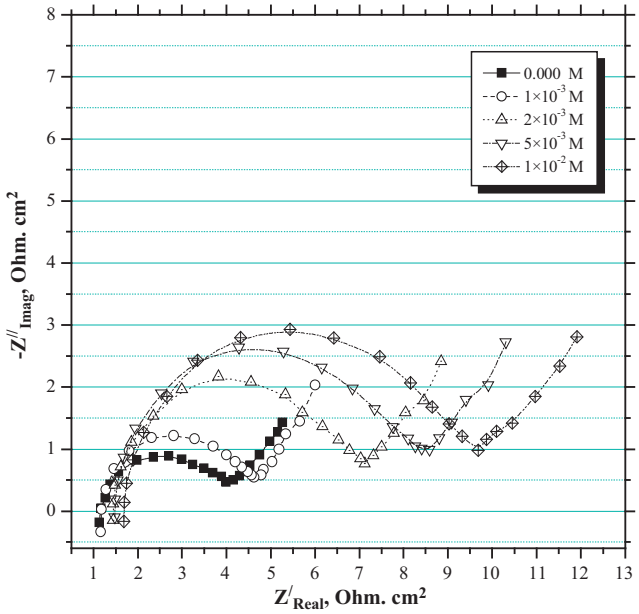

Fig. 12. Nyquist plot for pure zinc in 7 M KOH containing various concentrations of $K_3[Fe(CN)_6]$, measured at E_{corr}, Ac amplitude 5 mV, the frequencies from 100 kHz to 5 Hz, and at 25 °C.

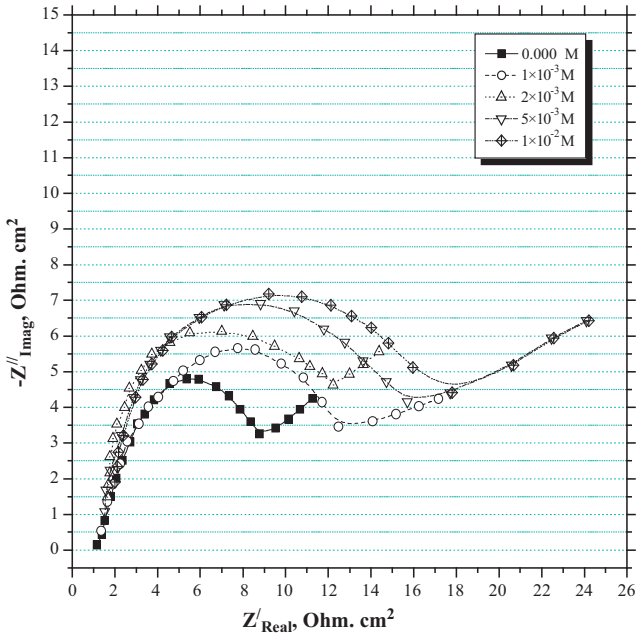

Fig. 13. Nyquist plot for Zn–0.5Ni alloy in 7 M KOH containing various concentrations of $K_3[Fe(CN)_6]$, measured at E_{corr}, Ac amplitude 5 mV, the frequencies from 100 kHz to 5 Hz, and at 25 °C.

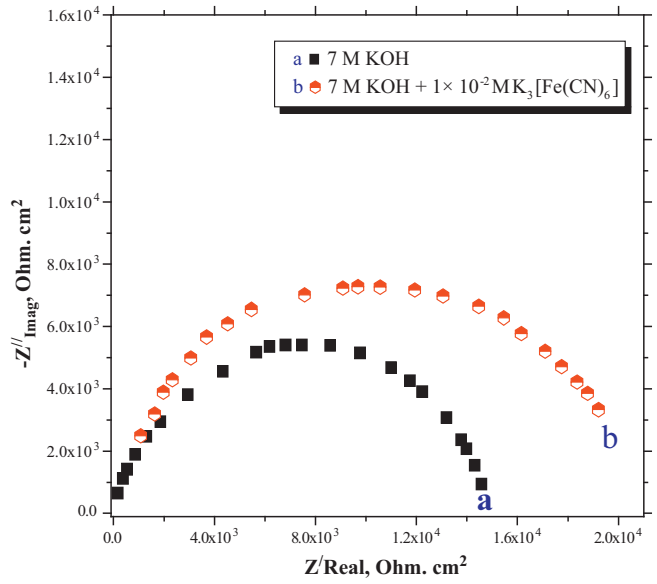

Fig. 15. Nyquist plot for oxide film formed anodically at 1.0 V vs. SCE on pure Zn in 7 M KOH solution in the absence and presence of 1×10^{-2} M $K_3[Fe(CN)_6]$, measured at E_{corr}, Ac amplitude 5 mV, the frequencies from 100 kHz to 5 Hz, and at 25 °C.

burg impedance (Z_w) increase while the capacity of the double layer (C_{dl}) decreases with increasing the inhibitor concentration (Table 2). This process may be argued to the inhibition of corrosion process, i.e. hydrogen evolution and dissolution of Zn or Zn–0.5Ni alloy as discussed above in both Tafel plot and potentiodynamic investigations. The equivalent circuit model used to fit the experimental data is shown in Fig. 14a as previously reported [17,41]. The measured complex-plane impedance plot is similar to that calculated by the equivalent circuit model. The charge transfer resistance (R_{ct}), the Warburg impedance (Z_w) and the capacity of the double layer (C_{dl} and $C_{inhibitor}$ in the absence and presence of the inhibitor, respectively) are determined by analysis of the complex-plane impedance plot and the equivalent circuit model. From the data obtained in Table 2, one can conclude that values of both R_{ct}, Z_w increase while C_{dl} (in the pure medium) decreases as an increase the inhibitor concentration ($C_{inhibitor}$), and this behavior is in good agreement with that obtained of the Tafel plot measurements. In other words, the corrosion inhibition strengthened with the increase of $[Fe(CN)_6]^{3-}$ complex anion concentration. It may result from the fact that adsorption amount and coverage of the inhibitor on the electrode surface increases with increasing concentration. It is worthy noting that, the presence of the inhibitor does not alter the profile of the impedance spectra, suggesting similar mechanisms for zinc and its alloy dissolution in KOH solution in the absence and presence of the inhibitor.

Figs. 15 and 16 show the complex-plan impedance diagram for zinc and its investigated alloy in 7 M KOH solution containing 1×10^{-2} M $K_3[Fe(CN)_6]$ which is formed in the passive region

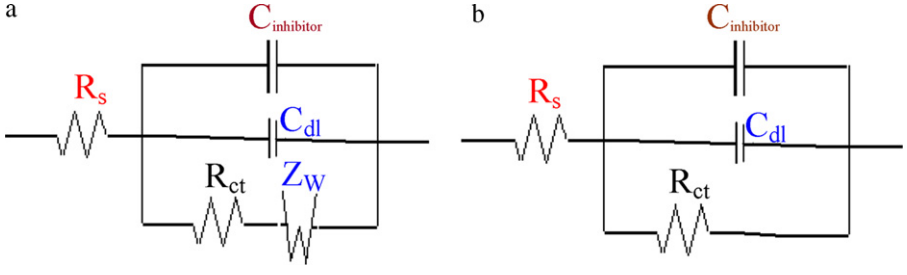

Fig. 14. Equivalent circuit model used in the fitting of impedance data of (a) semicircle with Warburg tail (b) semicircle without Warburg tail.

Table 2
Impedance parameters obtained for the corrosion of pure Zn and Zn–0.5Ni alloy in 7 M solution of KOH containing various concentrations of $K_3[Fe(CN)_6]$ at E_{corr} and 25 °C.

Metal and alloy	Pure Zn					Zn–0.5Ni alloy				
Concentration of $K_3[Fe(CN)_6]$ (mol/l)	R_S (Ω cm^2)	R_{ct} (Ω cm^2)	$C_{dl}/C_{inhbitor}$ (mFcm^{-2})	Z_w (Ω^{-1} s$^{1/2}$ cm^{-2})	IE (%)	R_s (Ω cm^2)	R_{ct} (Ω cm^2)	$C_{dl}/C_{inhbitor}$ (mFcm^{-2})	Z_w (Ω^{-1} s$^{1/2}$ cm^{-2})	IE (%)
00.00 M	1.08	6.0	31.0[a]	33	–	1.14	12.5	10.0[a]	79.5	–
1×10^{-3} M	1.15	8.30	22.10	56.5	28	1.27	18.9	6.50	113	34
2×10^{-3} M	1.36	10.60	17.23	86	43	1.53	24.20	4.90	154	49
5×10^{-3} M	1.48	15.75	13.90	117	62	1.89	39.60	3.70	197	69.0
1×10^{-2} M	1.69	23.91	9.45	142	75.0	2.10	54.91	2.75	245	78.0

[a] The capacity of the double layer (C_{dl}) without inhibitor.

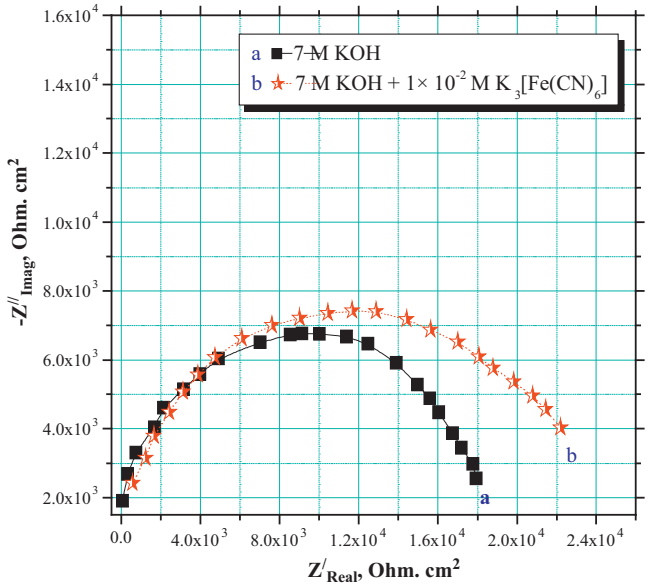

Fig. 16. Nyquist plot for oxide film formed anodically at +0.0 V vs. SCE on Zn–0.5Ni alloy in 7 M KOH solution in the absence and presence of 1×10^{-2} M $K_3[Fe(CN)_6]$, measured at E_{corr}, Ac amplitude 5 mV, the frequencies from 100 kHz to 5 Hz, and at 25 °C.

(at +1.0 and 0.0 V vs. SCE for Zn and alloy, respectively) at 25 °C. The data exhibited that a semicircle at the higher frequency, while at law frequency the Warburg Tail is disappeared. The equivalent circuit model for this system is shown in Fig. 14b. The measured complex-plane impedance plots are similar to those calculated by the equivalent circuit model [41]. This result means that the impedance has become capacitive. The semicircle diameter increases in the passivation potential region more than that in the active regions of both Zn and Zn–0.5Ni alloy. This result indicates that the charge transfer resistance (R_{ct}) is increased due to the formation of passive layer from the oxides film. On the other hand, the disappear of Warburg Tail at low frequency with increasing the applied potential in the positive direction (by comparison of Figs. 12 and 13 with Figs. 15 and 16) means that the diffusion species is strongly reduced. Therefore all the spectra show semicircle behavior in the passive region, quite characteristic for the pure kinetically controlled reaction [42]. On the other hand, addition of $[Fe(CN)_6]^{3-}$ complex anion (1×10^{-2} M) to KOH solution exhibited that the impedance becomes higher than that in the case of pure solution. This result may be due to the increasing of the passive layer thickness as a result of $[Fe(CN)_6]^{3-}$ adsorption on the surface. $[Fe(CN)_6]^{3-}$ complex anion incorporates into the oxide layer and block the pores present in the passive layer. This incorporation competes with OH^- ions into the passive layer and modifies its corrosion resistance, leading to a decrease in the corrosion rate [37]. These data are in a good agreement with the above results obtained by potentiodynamic and potentiostatic measurements.

Fig. 17(a) and (b) shows an EDX spectroscopy for zinc surface exposed to the passive film formed anodically at applied potential −0.50 V vs. SCE in 7 M KOH solution containing 1×10^{-2} M $K_3[Fe(CN)_6]$. In absence of $[Fe(CN)_6]^{3-}$ complex anion, Fig. 17a exhibits the characteristics peaks which are related to zinc, oxygen and potassium elements in pure 7 M KOH. This indicated that the corrosion product on Zn surface being ZnO. However, the data in Fig. 17b in the presence of 1×10^{-2} M $[Fe(CN)_6]^{3-}$ complex anion show additional peaks characteristic of Fe, C and N elements, and the lower peaks height of Zn than those observed in the absence of $[Fe(CN)_6]^{3-}$ complex anion. This result proved that the adsorption of $[Fe(CN)_6]^{3-}$ complex anion on Zn surface leads to a decrease

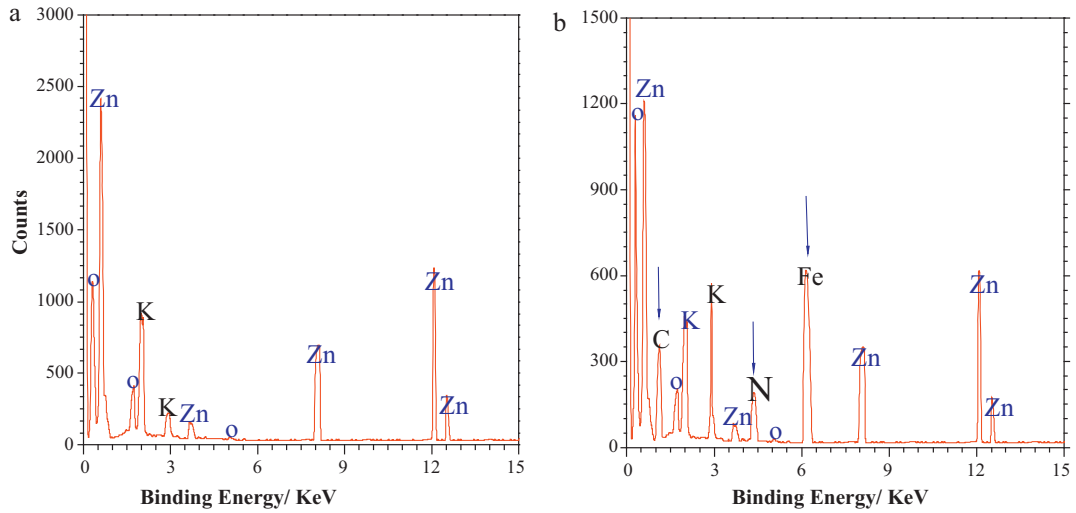

Fig. 17. EDX spectrum for the passive film on Zn metal surface formed anodically in (a) 7 M solution of KOH and (b) 7 M solution of KOH + 1×10^{-2} M $K_3[Fe(CN)_6]$ at applied potential −0.50 V vs. SCE.

of Zn oxide layer, and higher concentration of the inhibitor is necessary to delay the corrosion process.

Fig. 18(a)–(c) shows an SEM micrographs of the passive film formed on the Zn surface in the absence and presence of lower (1×10^{-3} M) and higher (1×10^{-2} M) concentrations of the investigated inhibitor. The results of SEM observed in the absence of $K_3[Fe(CN)_6]$ exhibited that thick porous layer of corrosion product (oxide film) covered most electrode surface. However, in the solution of the lower concentration of the inhibitor (1×10^{-3} M), the corrosion product is partially reduced as can be seen from the decrease of the oxide film (Fig. 18a). While in the solution containing higher concentration (1×10^{-2} M), almost no zinc oxide is formed. This suggests that the inhibitor is strongly adsorbed on Zn surface, and this hinders the corrosion process.

Fig. 19 is a complex-plane impedance diagram for Zn–0.5Ni alloy in 7 M KOH solution containing various concentrations of $[Fe(CN)_6]^{3-}$ complex anion, which is formed at certain positive potential (+0.425 V vs. SCE) and measured at E_{corr}. The results showed that a semicircle is observed at higher frequency, and the Warburg Tail at low frequency starts to appear again and increases with increasing the inhibitor concentration. This result shows that the impedance values decrease and capacity of the double layer increases as an increase the inhibitor concentration. This result may be interpreted by the increase of pore size in the passive layer, i.e. $[Fe(CN)_6]^{3-}$ complex anions interact with Ni species in the oxide layer, leading to formation of soluble complex diffuses to the bulk of solution. Therefore, OH^- ions reach the main alloy surface to begin new reactions. The reason behind this behavior may be that the oxide layer on the alloy surface becomes easily attacked by OH^- ion, and breakdown takes place. Hotellaz et al. [43] stated that the radius of Zn ions is higher than that of Ni (II), therefore Ni (II) can be precipitated in ZnO, and induces a lattice distortion. These results are in a good agreement with the above results obtained by potentiodynamic and potentiostatic measurements at the same mentioned potential.

Finally, one can conclude that the addition of $[Fe(CN)_6]^{3-}$ complex anions to KOH solution, can be considered as an important criteria for a good battery anode, due to its high negative open circuit potential, less corrosion rate and high self-catalysis in the passive region compared with those in its absence.

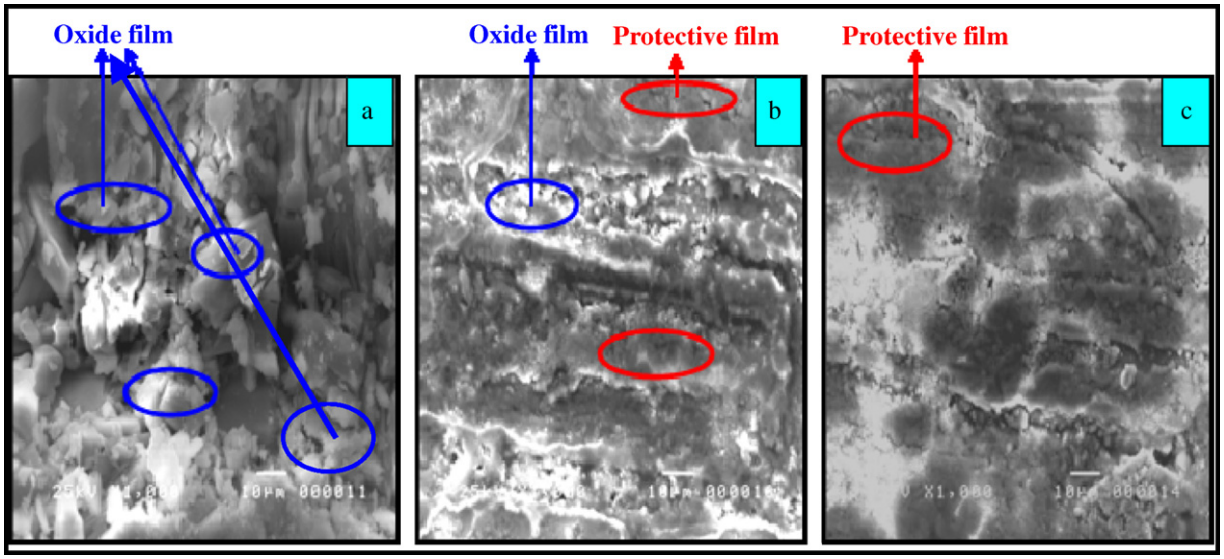

Fig. 18. SEM photographs (1000×) for the passive film on Zn metal surface formed anodically in (a) 7 M solution of KOH, (b) 7 M solution of KOH containing 1×10^{-3} M $K_3[Fe(CN)_6]$ and (c) 7 M solution of KOH containing 1×10^{-2} M $K_3[Fe(CN)_6]$ at applied potential −0.50 V vs. SCE.

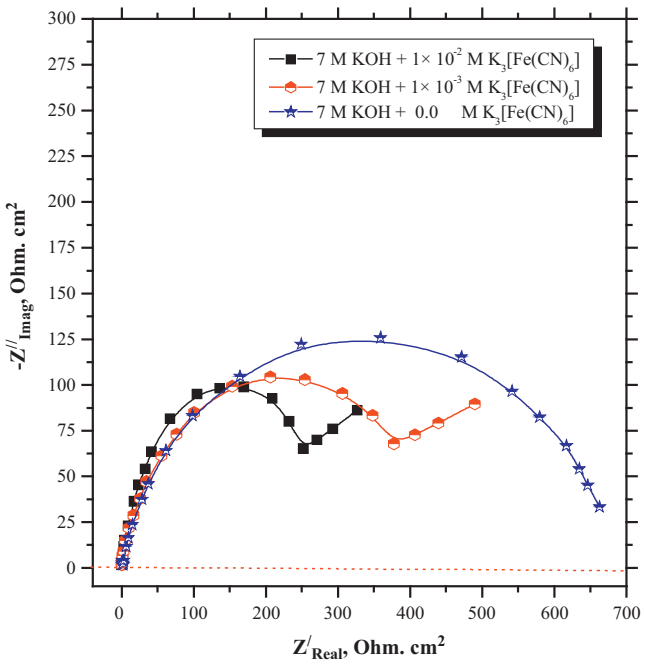

Fig. 19. Nyquist plot for oxide film formed anodically at the breakdown potential (0.425 V vs. SCE) on Zn–0.5Ni alloy in 7 M KOH solution containing various concentrations of $K_3[Fe(CN)_6]$, measured at E_{corr}, Ac amplitude 5 mV, the frequencies from 100 kHz to 5 Hz, and at 25 °C.

4. Conclusions

The following conclusions have been drawn from the present study:

1 The data of Tafel-plot are found to be in good agreement with electrochemical impedance spectroscopy (EIS) results that, the current density decreases and inhibition efficiency (*IE*%) increases as the concentration of the inhibitor is increased. However, the inhibition efficiency in the case of alloy is higher than that of pure zinc at the same examined concentrations. Therefore, pure zinc or Zn–0.5Ni alloy electrode in 7 M KOH with $[Fe(CN)_6]^{3-}$ complex anions provides a good combination of anode and electrolyte for use in alkaline batteries.

2 The potentiodynamic polarization curves exhibited that, addition of increasing concentration of the inhibitor causes gradually decrease in the height of peaks as well as the passivation current and shifts the peak potentials to more negative direction. This indicates that the presence of the inhibitor decreases the anodic dissolution, and hence improves its stability against corrosion.

3 The data exhibited that, potentiodynamic, potentiostatic and electrochemical impedance spectroscopy measurements are in a good agreement that, the breakdown of the oxide layer on the alloy surface increases with increasing the concentration of $[Fe(CN)_6]^{3-}$ complex anion. This behavior can be attributed to the dissolving power of oxide layer on the alloy surface occurs somewhat easier in the presence of the mentioned inhibitor. Therefore, the inhibitor has beneficial effect as self-catalysis for the studied alloy, which can be used as anodes in alkaline storage batteries.

4 Accordingly, it has been proved that it is possible to adding $K_3[Fe(CN)_6]$ to alkaline solution in the case of use pure zinc or Zn–0.5Ni alloy as a good anode in alkaline batteries.

5 Finally, one can conclude that the addition of $[Fe(CN)_6]^{3-}$ complex anion to KOH solution, can be considered as an important criteria for a good battery anode. This behavior is due to its high negative open-circuit potential, less corrosion rate and higher self-catalysis in the passive region compared with those in its absence.

References

[1] Y. Ein-Eli, M. Auinat, D. Starosvetsky, J. Power Sources 114 (2003) 330.
[2] K.V. Kordesch, Batteries, vol. 1, Marcel Dekker, New York, 1974, p. 324.
[3] T.D. Dirkse, R. Timmer, J. Electrochem. Soc. 116 (1969) 162.
[4] M. Meeus, Y. Strauven, L. Groothhaert, Extended Abstracts of the 15th International Power Sources Symposium, 1986, p. 1.
[5] L.Z. Vorkapic, D.M. Drazic, A.R. Despic, J. Electrochem. Soc. 121 (1974) 1385.
[6] M. Takahashi, Research report for zinc electrode in alkaline solution, 1985, The Electrochemical Society of Japan, 1986, p. 1.
[7] M. Yano, M. Nogami, I. Yonezu, K. Nishio, Y. Akai, M. Kurimura, Denki Kagaku 65 (1997) 154.
[8] M. Yano, Y. Akai, M. Kurimura, S. Fujitani, K. Nishio, Denki Kagaku 65 (1997) 650.
[9] M. Yano, Y. Akai, M. Kurimura, S. Fujitani, K. Nishio, J. Power Sources 74 (1998) 129.
[10] A. Miura, K. Takada, R. Okazaki, H. Ogawa, T. Uemura, Y. Nakamura, N. Kasahara, Denki Kagaku 57 (1989) 459.
[11] A. Miura, K. Takada, R. Okazaki, H. Ogawa, T. Uemura, Y. Nakamura, N. Kasahara, Extended Abstracts 55th Electrochemical Society of Japan, 1988, p. 16.
[12] A. Miura, Extended Abstracts of the Third Colloidal and Surface Chemistry Symposium in Japan, 1996, p. 66.
[13] K. Yamakawa, H. Tsubakino, K. Kawanishi, Denki Kagaku 59 (1991) 325.
[14] N. Kasahara, T. Uemura, A. Okada, Extended Abstracts 27th Battery Symposium in Japan, 1986, p. 7.
[15] T. Yamasoto, T. Uemura, M. Nakamura, N. Kasahara, A. Miura, K. Takada, R. Okazaki, H. Ogawa, Extended Abstracts 28th Battery Symposium in Japan, 1987, p. 37.
[16] J. Dobryszycki, S. Biallozor, Corros. Sci. 43 (2001) 1309.
[17] A. El-Sayed, H.S. Mohran, H.M. Abd El-Lateef, J. Power Sources 195 (2010) 6924.
[18] R. Sohr, L. Miller, R. Landsberg, J. Electroanal. Chem. 50 (1974) 55.
[19] P. Bindra, H. Gerischer, L.M. Peter, J. Electroanal. Chem. 57 (1974) 435.
[20] J. Kawiak, T. Jedral, Z. Galus, J. Electroanal. Chem. 145 (1983) 163.
[21] A.M.T. Oimedo, R. Perejro, D.J. Schiffrin, J. Electroanal. Chem. 74 (1976) 19.
[22] A. El-Sayed, Ann. Chim. 80 (1990) 283.
[23] A. El-Sayed, A.M. Shaker, H. Gad El-Kareem, Bull. Chem. Soc. Jpn. 76 (2003) 1527.
[24] A. El-Sayed, H.S. Mohran, H.M. Abd El-Lateef, Corros. Sci. 51 (2009) 2675.
[25] M.S. Abdel Aal, S. Radwan, A. El-Sayed, Br. Corros. J. 18 (1983) 25.
[26] R. Tremont, H. De Jesus-Cardona, J. Garcia-Orozco, R.J. Castro, C.R. Cabrera, J. Appl. Electrochem. 30 (2000) 737.
[27] J.W. Schultze, K. Wippermann, Electrochim. Acta 32 (1987) 823.
[28] M.S. Abdel Aal, A.A. Abdel Wahab, A. El-Sayed, Corrosion 37 (1981) 557.
[29] S.S. Abd El-Rehim, H.H. Hamdy, M.A. Amin, Corros. Sci. 46 (2004) 5.
[30] A. El-Sayed, A.M. Shaker, H.M. Abd El-Lateef, Corros. Sci. 52 (2010) 72.
[31] A. El-Sayed, H.S. Mohran, H.M. Abd El-Lateef, Corros. Sci. 52 (2010) 1976.
[32] R.V. Moshtev, Electrochim. Acta 16 (1971) 2039.
[33] S.S. Abd El Rehim, H.H. Hassan, N.F. Mohamed, Corros. Sci. 46 (2004) 1071.
[34] T.P. Hoar, D.C. Mears, G.P. Rothwell, Corros. Sci. 5 (1965) 279.
[35] B.F. Giannetti, P.T. Sumodjo, T. Rabockai, J. Appl. Electrochem. 20 (1990) 672.
[36] H.H. Hassan, S.S. Abd El-Rehim, N.F. Mohamed, Corros. Sci. 44 (2002) 37.
[37] W.A. Badawy, K.M. Ismail, A.M. Fathi, Electrochim. Acta 50 (2005) 3603.
[38] Electrochemical Methods, Fundamentals and applications, 2nd ed., Wiley, 2000.
[39] E. Barcia, O.R. mattos, N. Pebere, B. Tribollet, J. Electrochem. Soc. 140 (1993) 2825.
[40] C. Deslouis, B. Tribollet, C. Pagura, M.M. Musiani, J. Appl. Eleetrochem. 18 (1988) 374.
[41] A. El-Sayed, J. Appl. Electrochem. 27 (1997) 193.
[42] M. Metikoš-Huković, S. Omanović, J. Electroanal. Chem. 455 (1998) 181.
[43] B. Hotellaz, J.B. Bonino, A. rousset, J. Mater. Sci. 34 (1999) 881.